water

MDPI

Article

Optimisation and Modelling of Pb(II) and Cu(II) Biosorption onto Red Algae (*Gracilaria changii*) by Using Response Surface Methodology

Mubeen Isam *, Lavania Baloo *, Shamsul Rahman Mohamed Kutty and Saba Yavari

Department of Civil and Environmental Engineering, Universiti Teknologi PETRONAS (UTP), Bandar Seri Iskandar 32610, Perak Darul Ridzuan, Malaysia; shamsulrahman@utp.edu.my (S.R.M.K.); sabayavari2005@yahoo.com (S.Y.)

* Correspondence: mubeen.isam@gmail.com (M.I.); lavania.baloo@utp.edu.my (L.B.)

Received: 29 July 2019; Accepted: 17 August 2019; Published: 7 November 2019

Abstract: The removal of Pb(II) and Cu(II) ions by using marine red macroalgae (*Gracilaria changii*) as a biosorbent material was evaluated through the batch equilibrium technique. The effect of solution pH on the removal of metal ions was investigated within the range of 2–7. The response surface methodology (RSM) technique involving central composite design (CCD) was utilised to optimise the three main sorption parameters, namely initial metal ion concentration, contact time, and biosorbent dosage, to achieve maximum ion removal. The models' adequacy of response was verified by ANOVA. The optimum conditions for removal of Pb(II) and Cu(II) were as follows: pH values of 4.5 and 5, initial concentrations of 40 mg/L, contact times of 115 and 45 min, and biosorbent dosage of 1 g/L, at which the maximum removal percentages were 96.3% and 44.77%, respectively. The results of the adsorption isotherm study showed that the data fitted well with the Langmuir's model for Pb(II) and Cu(II). The results of the adsorption kinetic study showed that the data fitted well with the pseudo-second order model for Pb(II) and Cu(II). In conclusion, red alga biomass exhibits great potential as an efficient low-cost sorbent for removal of metal ions.

Keywords: biosorption; biomass; mathematical modelling; sorbent; isotherm; kinetics; optimization; response surface methodology; heavy metals; lead; copper

1. Introduction

Heavy metal-containing water is a severe pollution issue that considerably affects the environment and animal and human health. Heavy metals can accumulate in the food chain and cause major human health problems if not managed and treated properly. Kim et al. classified heavy metals into two groups based on their toxicity: essential and non-essential heavy metals [1]. Essential heavy metals including Cu, Fe, Co, and Zn are relatively less toxic at low concentration levels. They can act as cofactors in different biochemical and physiological functions in living organisms; however, they become toxic if they exceed the threshold level [2]. On the other hand, non-essential heavy metals including Pb, Cd, Hg, and As are highly toxic and can be lethal even at low concentrations. Heavy metals severely affect the human nervous system and can cause headache, hypertension, fatigue, anaemia, and even cancer [3,4]. Lead and Cu(II) are listed on the United States Environmental Protection Agency (USEPA) priority control pollutants list due to their persistence and irreversible toxic characteristics [1]. Rapid industrialisation increases the levels of heavy metal contamination in the environment [5,6]. Heavy metals are discharged from various industries such as those involving petroleum, mining, and electroplating (Table 1). If untreated, heavy metals can accumulate in the receiving environment and directly or indirectly enter the food chain [2,7,8]. According to the USEPA, the allowable levels of Pb(II) and Cu(II) in drinking water are 0.015 and 1.3 mg/L, respectively [9].

Table 1. Some of the major industrial sources for Pb(II) and Cu(II) (Adapted from Nagajyoti et al. [8]).

Element	Industries
Pb(II)	Metal plating, mining, battery manufacturers, automobile and petroleum industries
Cu(II)	Electroplating, chemical industries, dyes and pigments paper mills, textiles, and fertilizers

Different methods, such as ion exchange, chemical precipitation, membrane filtration, coagulation, and flocculation, have been used for removal of heavy metals from wastewater. These methods are either ineffective or expensive when heavy metals are present in low concentrations. Other limitations of such methods are the complexity of the operation and large area requirement [10]. Adsorption is considered as an effective and economic removal method for heavy metals in wastewater treatment. It offers simplicity and flexibility in both operation and design [6,11–13]. The utilization of biomaterials has many advantages over conventional methods, including low cost, minimization of chemical or biological sludge, the possibility of metal recovery, and the ability to regenerate bio sorbents [14]. A variety of adsorbents, like graphene oxide [15], the metal organic framework [15], zeolites [16,17], activated biochar [18], MXenes [19], carbon nanotubes [20], and activated carbon [21], etc., have been reported for the removal of heavy metals from aqueous solutions. However, it should be noted that compared to agricultural-based biosorbents, these adsorbents are often expensive. Biosorption of heavy metals is an alternative economical method [22,23]. The criteria for selection of the ideal biosorbent should include its availability, non-toxicity, cost, metal-binding capacity, and regeneration [24]. Biosorbents that require minimal processing or are abundant in nature are considered low-cost materials [25].

Macroalga biomass can potentially stabilise heavy metals due to their small uniform particle size and presence of different metal binding sites on their cell walls [26–30]. Red macroalgae (*Gracilaria changii*) are abundant in the coastal areas of Oceania, Africa, and Asia [31]. This seaweed species is the most abundant macroalgae in Malaysia [32–34]. The utilisation of such a biomass resource would provide a sustainable way to control biomass degradation in the environment and thus reduce the related eutrophication problem in the oceans [35]. This study aims to examine and optimise the performance of red macroalgae for the adsorption of Pb(II) and Cu(II) from aqueous solution through batch equilibrium procedure and response surface methodology (RSM).

RSM is a well-recognised mathematical and statistical tool that can be used to evaluate the effects of different factors on a response of interest. RSM is a powerful tool that measures regional optimal responses by using a sequence of designed experiments [36]. In general, several steps are followed to implement RSM, starting with the selection of independent variables that significantly affect the desired response. The next step is to select an experimental design and conduct the experiments. The third step is to statistically analyse the obtained data and fit them to a polynomial function. The fourth step is to evaluate the model's fit and finally determine the optimum values. RSM can be used to reduce the number of tests needed to find the optimum conditions. RSM consists of mathematical and statistical techniques based on fitting the experimental data with the empirical models. Central composite design (CCD) is the most commonly used experimental design performed within the experiment range [36,37]. The present study investigated the effects of four different adsorption factors, namely solution pH, initial metal ion, contact time, and biosorbent dosage, on removal of Pb(II) and Cu(II) ions. RSM was utilised to optimise the effects of initial metal ion, contact time, and biosorbent dosage on the biosorption process.

2. Materials and Methods

2.1. Collection, Purification, and Preparation of Red Alga Biomass

Red algae were collected from the Fishery Department of Langkawi. The biomass was washed repeatedly with tap water to remove any trapped impurities and rinsed with distilled water for additional purity. The washed biomass was sun dried for 2 days and oven dried at 70 °C for 24 h.

The dried algae were ground using a mill (FRITSCH cutting mill combination PULVERISETTE 25/19) (FRITSCH, Pittsboro, North Carolina, NC, USA). The obtained powder was sieved within the range of 0.15–0.30 mm and stored in airtight bottle.

2.2. Alga Biomass Characterisation

Field-emission scanning electron microscopy with energy-dispersive X-ray (FESEM-EDX) spectroscopy (Carl-Zeiss AG, Oberkochen, Germany) was used to study the surface morphology of the biosorbent and its component. The biosorbent was subjected to analysis by the instrument before and after the biosorption of Pb(II) and Cu(II).

Fourier transform infrared (FTIR) spectroscopy (Perkin – Elmer, Waltham, Massachusetts, MA, USA) was used to detect changes in the vibration frequency in the biosorbent before and after biosorption. Infrared spectra were recorded within the range of 550–4000 cm^{-1}. The spectral data were processed using Essential FTIR v3.5 (Operant LLC, Madison, Wisconsin, WI, USA).

2.3. Preparation of Synthetic Solution

Stock solutions of metals (1000 mg/L) were prepared by dissolving 1.598 g of $Pb(NO_3)_2$ or 3.802 g of $Cu(NO_3)_2{\cdot}3H_2O$ in 1 L of distilled water. The stock solutions were diluted to obtain different concentrations.

2.4. Batch Biosorption Experiment

All adsorption tests were carried out in 250 mL conical flasks containing 100 mL of each Pb(II) and Cu(II) solution. The tests were conducted by varying four factors, namely, pH (2–7), initial concentration (10, 40, 70, 100, and 130 mg/L), contact time (10, 45, 80, 115 and 150 min), and biomass dosage (0.1, 0.4, 0.7, 1, and 1.3 g/L), on metal biosorption. All the samples were agitated at 180 rpm at room temperature in orbital shaker (Protech model 722). Samples were collected at the predetermined interval and filtered through filter paper (Whatman No.1, 0.45 μm). The filtrates were examined for metal ion concentration by using flame atomic absorption spectrophotometer (AAS) model (Agilent 200 series AA systems, 240FS AA, Agilent technologies, Santa Clara, California, CA, USA). A similar procedure proposed by Lingamdinne was conducted for removal of metal ions [38]. The experiments were conducted in triplicate to increase the precision and minimise error. Removal percentage was calculated using Equation (1) [39]:

$$Removal\ \% = 100\ \times \left(C_0 - C_f\right)/C_0 \tag{1}$$

where C_0 and C_f are the initial and final metal ion concentrations, respectively.

2.5. Design of Experiment

2.5.1. Effect of Solution pH

The effect of solution pH on the removal of metal ions was investigated by varying the pH within 2–7 while maintaining the ion concentration, contact time and dosage at 100 mg/L, 120 min and 1 g/L, respectively. The solution pH was adjusted by adding NaOH and HCl solutions. After shaking, the samples were filtered and examined using AAS.

2.5.2. Experimental Design Using RSM

RSM was used to design the experiment to model and evaluate the effects of three independent variables (A: ion initial concentration, B: contact time and C: biosorbent dosage) on the response (R: metal removal percentage). Full factorial CCD was implemented. The CCD for the three independent variables was based on six axial points, eight factorial points and six replicates at the central point.

The selected factors were varied at five levels (−α, −1, 0, 1, +α). The number of experiment runs was calculated based on Equation (2):

$$N = 2^K + 2K + C = 2^3 + 2 \,.\, 3 + 6 = 20 \tag{2}$$

where N is the number of runs, K is the number of factors to be tested, and C is the number of experiments conducted at the centre. The lower and higher limits of each factor are shown in Table 2. The experiment data matrix was determined using State–Ease design expert v10.0.1. The obtained model was statistically analysed using analysis of variance (ANOVA). The interactions between variables were studied using surface contour plots.

Table 2. Ranges and levels of independent variables.

Independent Variable	Ranges and Coded Levels				
	−α	**−1**	**0**	**+1**	**+α**
Initial concentration (mg/L)	10	40	70	100	130
Contact time (min)	10	45	80	115	150
Adsorbent dosage (g/L)	0.1	0.4	0.7	1	1.3

2.6. Adsorption Isotherms

Adsorption isotherm models were utilised to examine the adsorption behaviour of metal ions on the adsorbent. Langmuir and Freundlich isotherms are the most commonly used in exploring the adsorption behaviour of metal ions. The Langmuir model assumes that the adsorption is a monolayer type and occurs on a homogeneous surface with a finite number of active sites, regardless of the existence of mutual interaction between the adsorbent molecules [40]. The linearized Langmuir equation can be written in the following form:

$$\frac{C_e}{q_e} = \frac{1}{K_L} \times \frac{1}{q_m} + C_e \frac{1}{q_m} \tag{3}$$

where C_e (mg/L) is the equilibrium concentration, and q_e (mg/g) is the amount of the adsorbed ion; q_m (mg/g) and K_L (L/mg) are the maximum adsorption capacity and rate of adsorption (Langmuir constant), respectively.

One of the essential characteristics of Langmuir isotherm modelling is the term of equilibrium dimensionless parameter (R_L), which can be calculated using Equation (4):

$$R_L = \frac{1}{1 + K_L C_0} \tag{4}$$

where K_L (L/mg) and C_0 (mg/L) are the Langmuir constant and initial ion concentration, respectively. The R_L value determines whether the adsorption is unfavourable ($R_L > 1$), favourable ($0 < R_L < 1$), linear ($R_L = 1$), and irreversible ($R_L = 0$) [41].

The Freundlich model presumes that molecules are adsorbed on the heterogeneous surfaces based on different energy sites. The model considers the mutual interaction between adsorbate molecules. The linear form of the Freundlich equation can be used in the following form:

$$\log q_e = \log K_F + \frac{1}{n} \log C_e \tag{5}$$

where K_F [(mg/g)/(L/mg)$^{1/n}$] and $1/n$ are Freundlich constants related to capacity and favourability of the adsorption, respectively. The values of $1/n$ within 0 and 1 indicate favourable adsorption. n represents the intensity of adsorption.

2.7. Adsorption Kinetics

Adsorption kinetics models were utilised to examine to study the effect of contact time between adsorbent and adsorbate. The adsorption kinetics can strongly constrain the use of some adsorbents [42]. Small adsorption kinetics leads to longer adsorption process time which can cause the adsorption to be inadequate [42]. In this study. Four different kinetics models were investigated, namely the pseudo-first-order, pseudo-second order, the Elovich, and the intra-particle diffusion kinetic models, and were used to test the experimental data.

The pseudo-first -order model is suitable for low concentration of adsorbate [43]. The linearized form on this model can be expressed as follows:

$$\log(q_e - q_t) = \log(q_e) - k_1 t \tag{6}$$

where q_e and q_t is the metal uptake of *G. changii* at equilibrium and at time t, respectively, and k_1 is the pseudo-first order model constant.

The linearized form of pseudo-second-order model can be expressed as follows [42]:

$$\frac{t}{q_t} = \frac{1}{q_e K_2} + \frac{1}{q_e}\, t \tag{7}$$

where q_e and q_t is the metal uptake of *G. changii* at equilibrium and at time t, respectively, and K_2 is the pseudo-second order model constant.

The Weber–Morris diffusion kinetic model was applied to the experimental data using the following form:

$$q_t = k_i t^{0.5} + C \tag{8}$$

where q_t is the metal uptake of *G. changii* at time *t* (mg/g) and k_i is the diffusion rate constant (mg/g min$^{0.5}$). The Elovich kinetic model simplified equation can be written in the following form [44]:

$$q_t = \frac{1}{\beta} \ln \alpha\beta + \frac{1}{\beta} \ln t \tag{9}$$

where α and β are the initial adsorption rage (mg/g min) and desorption constant (g/mg), respectively, and q_t is the metal uptake of *G. changii* at time *t* (mg/g).

3. Results

3.1. FESEM–EDX Analysis

The surface morphology and elemental composition of the biomass before and after the biosorption were investigated using FESEM-EDX. Figure 1 shows the surface morphology of red algae before and after the biosorption of Pb(II) and Cu(II). The morphological characterization of *G. changii* after the biosorption of Pb(II) and Cu(II) was significantly different from those before biosorption. The pores on the biomass surface became smooth after the biosorption. This change can be explained by accumulation of metal ions on the surface by electrostatic attraction effect, which has been reported previously by [6,45].

The EDX analysis showed the biosorbent surface elemental composition before and after the biosorption. The system was calibrated using $CaCO_3$ (C), SiO_2 (Si), MAD-10 Feldspar (K), FeS_2 (S), Wollastonite (Ca), KCl (K), MgO (Mg), Mn (Mn), PbF_2, and Cu as standards. The Pb-Mα peak was recorded at 2.342 KeV overlapping with S-Kα peak at 2.304, the Pb-L peak at 10.55 was also recorded. The Cu-Kα and Cu-Lα peaks were recorded at 8.04 and 0.93 KeV, respectively. The presence of Pb(II) (wt% = 7.83%) and Cu(II) (wt% = 2.94%) on the surface of the biomass after biosorption confirmed the attachment of the metal ions on the biosorbent surface. It was observed that amount of Mn, Mg, and K decreased or disappeared after the biosorption process. This change demonstrates a possible ion

exchange has occurred during the biosorption of Pb(II) and Cu(II). Similar observations were reported by [46–48]. Elemental mapping was carried out to show the spatial distribution of each element detected in EDX. All elements were recorded from their K_α line, except Pb, which was recorded from its Lα line (Figures S1–S3).

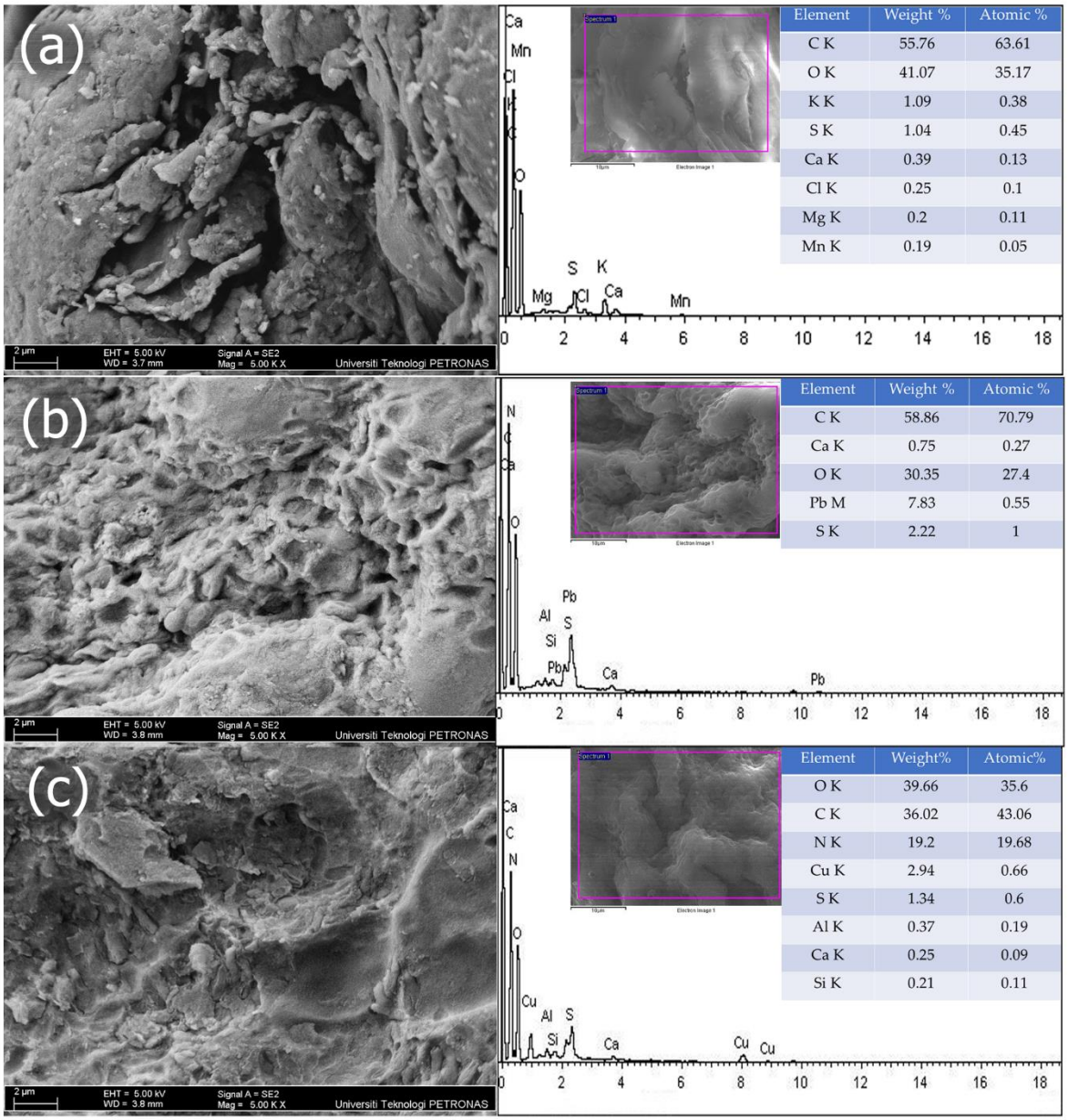

Element	Weight %	Atomic %
C K	55.76	63.61
O K	41.07	35.17
K K	1.09	0.38
S K	1.04	0.45
Ca K	0.39	0.13
Cl K	0.25	0.1
Mg K	0.2	0.11
Mn K	0.19	0.05

Element	Weight %	Atomic %
C K	58.86	70.79
Ca K	0.75	0.27
O K	30.35	27.4
Pb M	7.83	0.55
S K	2.22	1

Element	Weight%	Atomic%
O K	39.66	35.6
C K	36.02	43.06
N K	19.2	19.68
Cu K	2.94	0.66
S K	1.34	0.6
Al K	0.37	0.19
Ca K	0.25	0.09
Si K	0.21	0.11

Figure 1. Field-emission scanning electron microscopy (FESEM) images (**left**) and energy-dispersive X-ray (EDX) spectrums (**right**) for (**a**) unloaded biomass, (**b**) Pb(II)-loaded biomass, and (**c**) Cu(II)-loaded biomass.

3.2. FTIR Analysis

The functional groups on the biosorbent surface and their interaction during the biosorption process of Pb(II) and Cu(II) were investigated through FTIR spectrum analysis. Figure 2 shows the peaks corresponding to the functional groups of red algae before and after the biosorption of metal ions. The broad and strong peak at 3281.88 cm^{-1} was assigned to the overlapping of O–H and N–H stretching, indicating the existence of hydroxy stretching and carboxylic groups on the surface on algae [22,49]. The peak at 2928.35 cm^{-1} was attributed to the C–H stretching vibration of aliphatic groups [6,50].

The peaks at 1636.14 and 1545.21 cm^{-1} represented the presence of C=C stretching [51]. The peak found at 1413.01 cm^{-1} was assigned to the C–H bonding [50]. The peaks observed at 1243.88 cm^{-1} was attributed to the C–O stretching [45]. The sulfoxide band was assigned to the peak observed at 1030.15 cm^{-1} [52,53]. The numerous characteristic peaks observed on the surface indicate the complex nature of the biosorbent. The changes in vibration peaks are summarised in Table 3. The changes in the vibrational frequency of the functional groups after the biosorption of Pb(II) and Cu(II) indicated the involvement of these groups in the biosorption [6,54]. The difference in ion biosorption can be attributed to the different ions' affinity to for the functional groups [45].

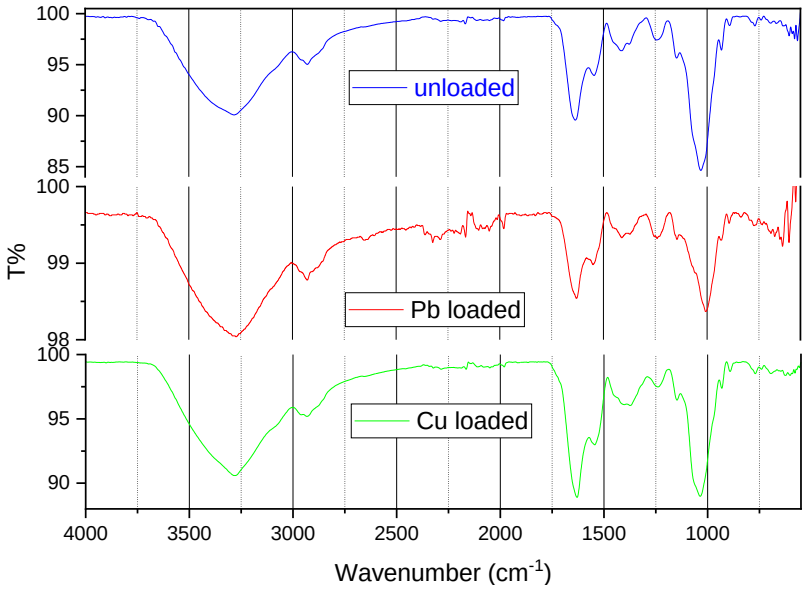

Figure 2. Fourier transform infrared (FTIR) image of red algae surface before and after biosorption of Pb(II) and Cu(II).

Table 3. Infrared vibration wavenumber and functional groups observed on unloaded, Pb(II), and Cu(II)-loaded biomass.

Wavenumber (cm^{-1})					Functional Groups
Unloaded Biomass	Pb(II) Loaded	Cu(II) Loaded	Difference after Pb(II) Biosorption	Difference after Cu(II) Biosorption	
1030.1515	1006.9091	1036.0909	23.2424	5.9394	S=O stretching
1243.8889	1241.3535	1239.1919	2.5354	4.697	C–O stretching
1413.0101	1411.6869	1401.9495	1.3232	11.0606	C–H stretching
1545.2121	1550.0505	1544.8687	4.8384	0.3434	C=C stretching
1636.1515	1630.1111	1629.9293	6.0404	6.2222	Asymmetric C=C stretching
2928.3535	2928.6263	2932.7879	0.2728	4.4344	–C–H stretching
3281.8889	3271.0909	3279.1515	10.798	2.7374	O–H stretching and N–H stretching vibration

3.3. *Effect of Solution pH*

Solution pH is a crucial factor that affects the biosorption of heavy metals. pH affects the metal ion chemistry in solution and the surface chemistry of the biosorbent [55,56]. The results obtained at pH values higher than 5.5 were ignored due to metal precipitation that formed metal hydroxides. These observations are similar to those reported by Sheng et al. [57] and Jalali et al. [58]. Therefore, the high removal percentage of over 5.5 is mainly due to the incorporating role of metal precipitation and adsorption [59]. A low removal percentage was observed at low pH. This finding might be due to proton H^+ competition with the metals' cations for the adsorption sites [60]. The increase in the removal percentage at pH higher than 5.5 could be attributed to the precipitation of metal

hydroxide [58]. The maximum removal percentages were 60% and 22% at pH 4.5 and 5 for Pb(II) and Cu(II), respectively. Similar results were obtained for Pb(II) and Cu(II) removal by using different types of macroalgae, including *Gracilaria corticate* [58], *Gracilaria canaliculate* [58], *Spirogyra* spp. [61], *Cladophora* spp. [61], and *Gelidium sesquipedale* [62]. Figure 3 shows the effect of solution pH on the removal percentages of Pb(II) and Cu(II).

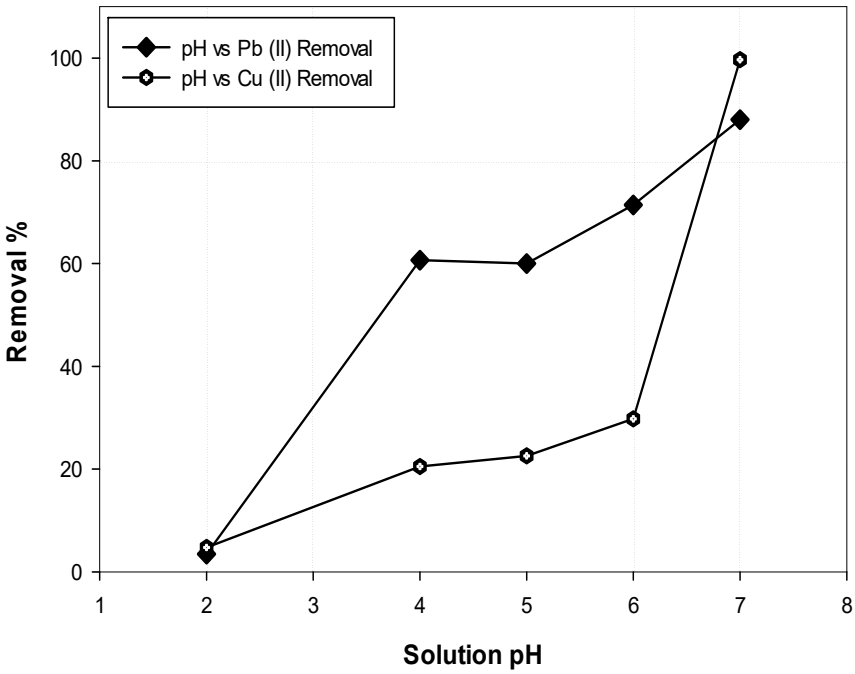

Figure 3. Pb(II) and Cu(II) removal percentage against solution pH.

3.4. Model Development for Pb(II) and Cu(II) Removal

A CCD matrix was used to investigate the interaction effects of three important factors, including metal ion concentration, contact time, and biosorbent dosage, on the removal of Pb(II) and Cu(II). The experimental design and the responses are shown in Table 4. Based on the obtained results, the following polynomial equations for Pb(II) and Cu(II) removal were developed:

$$\begin{aligned} Pb\ (II)\ Removal\ \ \% \\ &= 59.67 - 19A + 1.4B + 17.76C + 3.8AB - 3.88AC - 2.45\,BC + 1.71A^2 \\ &+7.7\,A^2B\ - 13.43\,A^2 \end{aligned} \tag{10}$$

$$\begin{aligned} Cu\ (II)\ Removal\ \ \% \\ &= 19.9 - 9.82A + 0.14B + 7.95C + 0.3AB - 3.13AC + 0.095BC + 3.25A^2 \\ &+0.26B^2 - 0.29C^2 \end{aligned} \tag{11}$$

where A, B, and C are the coded values for the selected influential parameters, namely, metal ion concentration, contact time and adsorbent dosage, respectively. Table 5 shows the ANOVA for the polynomial equations and the corresponding regression coefficients for the removal models of Pb(II) and Cu(II). The significance of the obtained models can be determined based on the p-value, the correlation of determination (R^2), and the results of the lack of fit test [36]. Both models showed p-values less than 0.0001, suggesting their significance. The lack of fit test showed the variation of responses around the fitted model. The insignificant lack of fit indicated that the model did not fit the data well. The model fit the real data better for Cu(II) than for Pb(II). The values of R^2 and adjusted R^2 were higher than 0.99 for Cu(II), whereas those for Pb(II) were lower at 0.97 and 0.95, respectively.

The coefficient of variance (CV) refers to the ratio of standard deviation to mean. The CV values were 7.9 and 3.26 for Pb(II) and Cu(II) models, respectively. A model is reproducible if the CV value is less than 10 [63]. Adequate precision (AP) is defined as the ratio of signal to noise [64]. An AP ratio higher than 4 is desired. The AP values of the models were 22.135 and 80.572 for Pb(II) and Cu(II), respectively, which showed a good signal and indicated that the models can be used to navigate the design space.

Table 4. Experimental design for biosorption of Pb(II) and Cu(II) on *Gracilaria changii*. CCD: central composite design.

RUN	Independent Factors			Responses		CCD Position
	Initial Concentration, *A*	Contact Time, *B*	Adsorbent Dosage, *C*	Pb(II) Removal%	Cu(II) Removal%	
1	10	80	0.7	95.70	75	Axial
2	40	115	0.4	87.70	21.63	Factorial
3	40	45	0.4	69.30	22.39	Factorial
4	40	115	1	96.30	44.82	Factorial
5	40	45	1	93.50	44.77	Factorial
6	70	80	0.7	67.79	19.63	Central
7	70	80	0.7	69.14	20.66	Central
8	70	80	0.7	62.46	19.93	Central
9	70	80	0.7	61.37	19.67	Central
10	70	80	0.1	15.70	2.93	Axial
11	70	80	0.7	55.84	20.26	Central
12	70	10	0.7	54.06	20.11	Axial
13	70	80	1.3	86.74	33.48	Axial
14	70	80	0.7	58.48	19.69	Central
15	70	150	0.7	59.67	20.71	Axial
16	100	115	0.4	57.22	9.23	Factorial
17	100	115	1	56.10	19.46	Factorial
18	100	45	1	32.30	18.64	Factorial
19	100	45	0.4	29.39	8.36	Factorial
20	130	80	0.7	29.61	12.55	Axial

Table 5. Analysis of variance (ANOVA) for Pb(II) and Cu(II) biosorption models.

Response	Source	Sum of Squares	df	Mean Square	F Value	*p*-Value Prob > F	Comments
Pb(II) Removal (%)	Block	325.79	1	325.79			SD = 4.89
	Model	9488.33	9	1054.26	44.01	<0.0001	Mean = 61.92
	A, initial concentration	5775.00	1	5775.00	241.06	<0.0001	CV = 7.90
	B, time	15.72	1	15.72	0.66	0.4389	R^2 = 0.977
	C, dosage	2523.21	1	2523.21	105.33	<0.0001	$R^2_{(adj)}$ = 0.9556
	AB	115.73	1	115.73	4.83	0.0555	AP = 22.135
	AC	120.14	1	120.14	5.01	0.0519	
	BC	48.13	1	48.13	2.01	0.1900	
	A^2	77.75	1	77.75	3.25	0.1051	
	A^2B	237.28	1	237.28	9.90	0.0118	
	A^2C	721.92	1	721.92	30.13	0.0004	
	Residual	215.61	9	23.96			
	Lack of fit	167.75	5	33.55	2.80	0.1697 [n]	
	Pure error	47.85	4	11.96			

Table 5. *Cont.*

Response	Source	Sum of Squares	df	Mean Square	F Value	*p*-Value Prob > F	Comments
Cu(II) Removal (%)	Block	67.24	1	67.24			SD = 0.69
	Model	1931.73	9	214.64	457.06	<0.0001 [s]	Mean = 21.00
	A, Initial concentration	801.85	1	801.85	1707.50	<0.0001 [s]	CV = 3.26
	B, time	0.30	1	0.30	0.64	0.4468 [n]	R^2 = 0.9981
	C, dosage	1010.96	1	1010.96	2152.78	<0.0001 [s]	$R^2_{(adj)}$ = 0.9959
	AB	0.72	1	0.72	1.54	0.2500 [n]	AP = 80.572
	AC	78.56	1	78.56	167.28	<0.0001 [s]	
	BC	0.072	1	0.072	0.15	0.7063 [n]	
	A^2	128.98	1	128.98	274.65	<0.0001 [s]	
	B^2	1.61	1	1.61	3.43	0.1010 [n]	
	C^2	1.90	1	1.90	4.04	0.0793 [n]	
	Residual	3.76	8	0.47			
	Lack of fit	2.92	4	0.73	3.47	0.1279 [n]	
	Pure error	0.84	4	0.21			

[S]: significant; [n]: insignificant; df: degree of freedom; SD: standard deviation; CV: coefficient of variance; R^2: correlation of determination; AP: adequate precision.

3.5. Effect of Factors on the Removal Percentages of Pb(II) and Cu(II)

Three-dimensional surface plots present the effects and interactions of independent variables, namely, ion concentration, contact time, and biosorbent dosage, on the removal percentages of Pb(II) (Figure 4) and Cu(II) (Figure 5) as the responses. The interaction of initial ion concentration and biosorbent dosage shown in Figures 4b and 5b indicates the significant influence of both factors on the removal of Pb(II) and Cu(II). For both adsorbates, the removal percentages increased with increasing biosorbent dosage. This result was due to the presence of additional active sites and large biosorbent surface area that is readily available for adsorption [65]. The removal percentage was reduced by increasing the initial ion concentration. This finding might be due to the limited active sites on the biosorbent surface at high adsorbate concentrations [66]. The removal percentage was increased slightly by increasing the residence time from 40 min to 115 min. These results confirmed that the initial adsorption rate was very rapid due to the availability of large surface area and the presence of unused sites on the biosorbent surface [38]. The slowing down of ion removal might be due to the difficulty of reaching the remaining vacant sites. Repulsive forces can also be a factor in this case. The efficiency of different macroalga species in metal ion adsorption has been reported [54,67,68]. The optimum values of the operation variables and the predicted maximum responses are presented in Table 6. The maximum removal percentages for Pb(II) and Cu(II) were predicted to be 91% and 44%, respectively. Verification experiments were conducted under the optimum conditions, and the removal percentages were 96% and 44% for Pb(II) and Cu(II), respectively; these findings are similar to the predicted values and indicated the suitability and accuracy of the suggested models. The diagnostic plots of the predicted versus actual values for Pb(II) and Cu(II) removal percentages are presented in Figure 6. The metal uptakes obtained under the optimum conditions were 38.52 and 17.9 mg/g for Pb(II) and Cu(II), respectively. Table 7 lists the comparison of metal uptake of Pb(II) and Cu(II) onto various types of algae.

Table 6. Predicted and experimental maximum values of Pb(II) and Cu(II) removal percentages achieved in optimum conditions.

Heavy Metal	Initial Concentration (mg/L)	Contact Time (min)	Adsorbent Dosage (g/L)	Removal%		Desirability
				Predicted	Experimental	
Pb(II)	40.000	115.000	1.000	91.425	96.3	0.940
Cu(II)	40.000	45.000	1.000	44.088	44.77	0.982

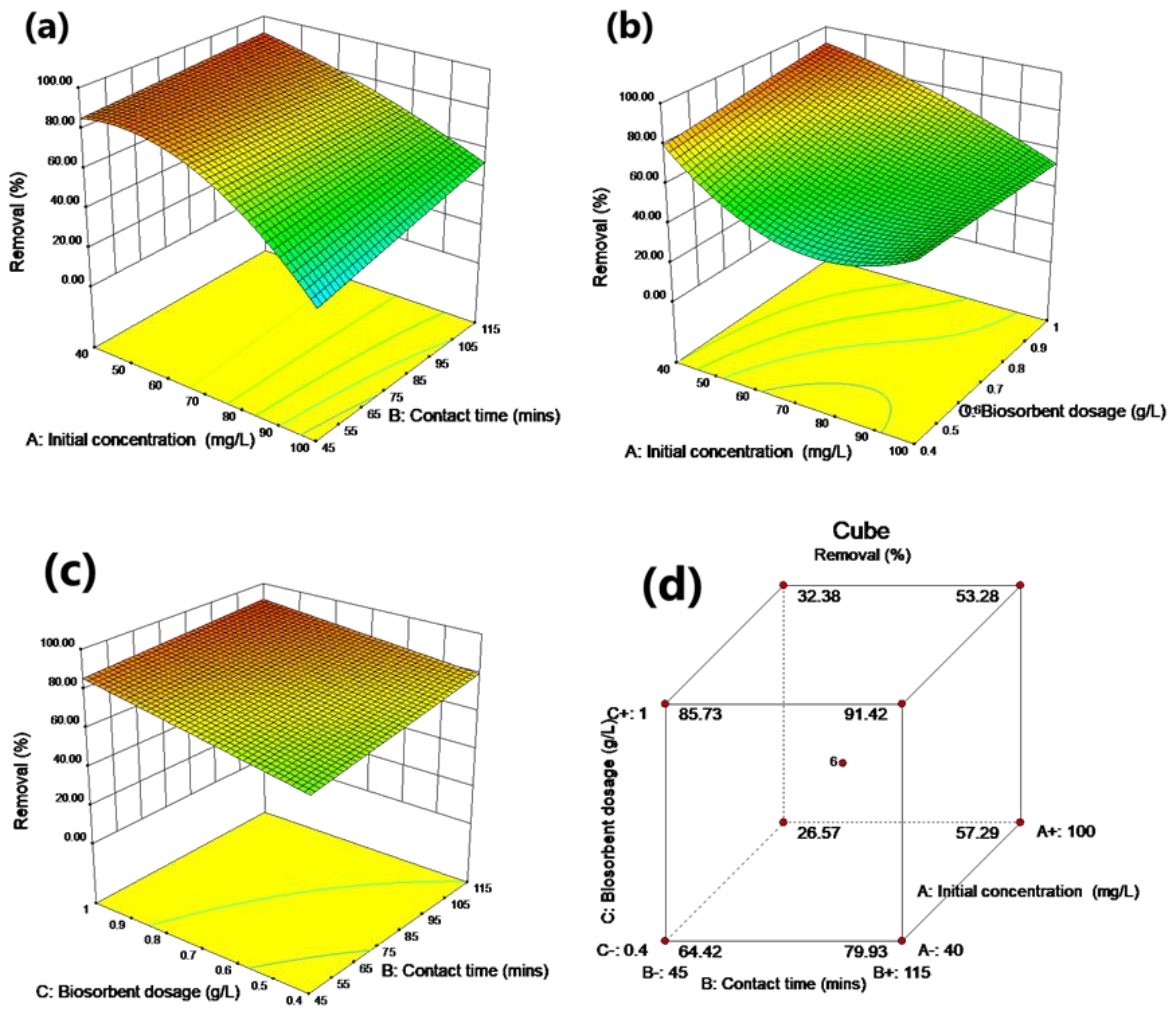

Figure 4. Combined effect of process variables (**a**) initial concentration and contact time, (**b**) initial concentration and biosorbent dosage, (**c**) contact time and biosorbent dosage on Pb(II) removal with interaction effect of dual factors, (**d**) removal percentage at each factorial point.

Table 7. Comparison between metal uptake of various types of algae.

Algae	Cu(II) Uptake (mg/g)	Pb(II) Uptake (mg/g)	References
Gracilaria corticata	NA	53.87	[58]
Gracilaria canaliculata	NA	41.44	[58]
Gracillaria sp.	NA	93.24	[57]
Asparagopsis armata	20.97	62.16	[69]
Chondrus crispus	40.03	203.06	[69]
Jania rubens	NA	29.00	[55]
Pterocladia capillacea	NA	33.15	[55]
Fucus spiralis	69.90	203.05	[69]
Ascophyllum nodosum	57.83	178.19	[69]
Sargassum sp.	62.91	240.35	[57]
Padina sp.	72.44	259.00	[57]
G. changii	17.90	38.52	Current study

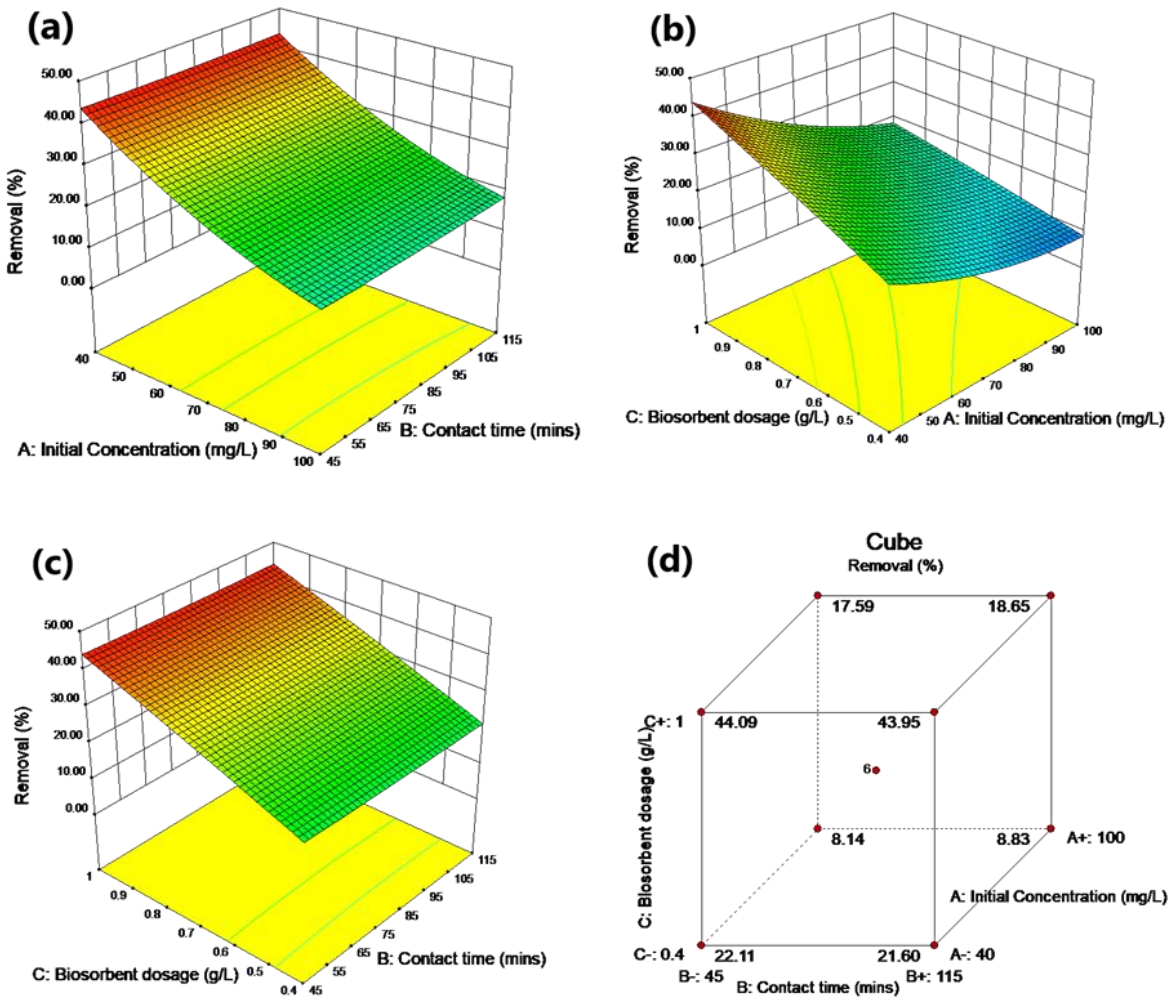

Figure 5. Combined effect of process variables (**a**) initial concentration and contact time, (**b**) initial concentration and biosorbent dosage, (**c**) contact time and biosorbent dosage on Cu(II) removal with interaction effect of dual factors, (**d**) removal percentage at each factorial point.

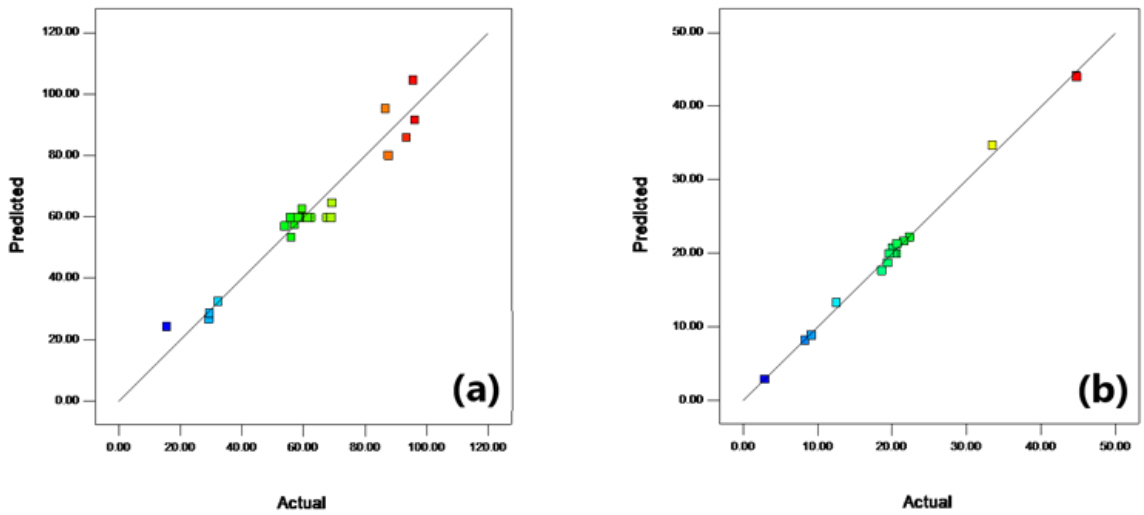

Figure 6. Diagnostic plots of predicted versus actual values for removal percentages of (**a**) Pb(II) and (**b**) Cu(II).

3.6. Adsorption Isotherm Study

The sorption equilibrium data were tested with the Langmuir and Freundlich isotherms. The model parameters for each isotherm and their respected correlation coefficients (R^2) are shown in Table 8. Figure 7 illustrates the Freundlich and Langmuir adsorption isotherms of ions on the biosorbent. The Langmuir isotherm best fitted for Pb(II) and Cu(II) on the red algae, with R^2 greater than 0.99. This fitting indicated that the sorption of both metal ions had a mono layer coverage on the sorbent surface [54]. The maximum sorption capacity was higher for Pb(II) than that for Cu(II). The K_L value of Pb(II) was higher than that of Cu(II), indicating the higher affinity of the former to the bonding sites on the alga surface. The values of R_L were 0.056 and 0.108, confirming the favourable sorption of Pb(II) and Cu(II) onto the alga biomass [70].

Table 8. Langmuir and Freundlich isotherm constants for Pb(II) and Cu(II).

Heavy Metal	Langmuir Isotherm Coefficient				Freundlich Isotherm Coefficient		
	q_m (mg/g)	K_L (L/mg)	R^2	R_L	K_F [(mg/g)/(L/mg)]$^{1/n}$	$1/n$	R^2
Pb(II)	62.89	0.42	0.9998	0.056	28.98	0.228	0.9614
Cu(II)	21.27	0.206	0.9992	0.108	11.975	0.1233	0.9415

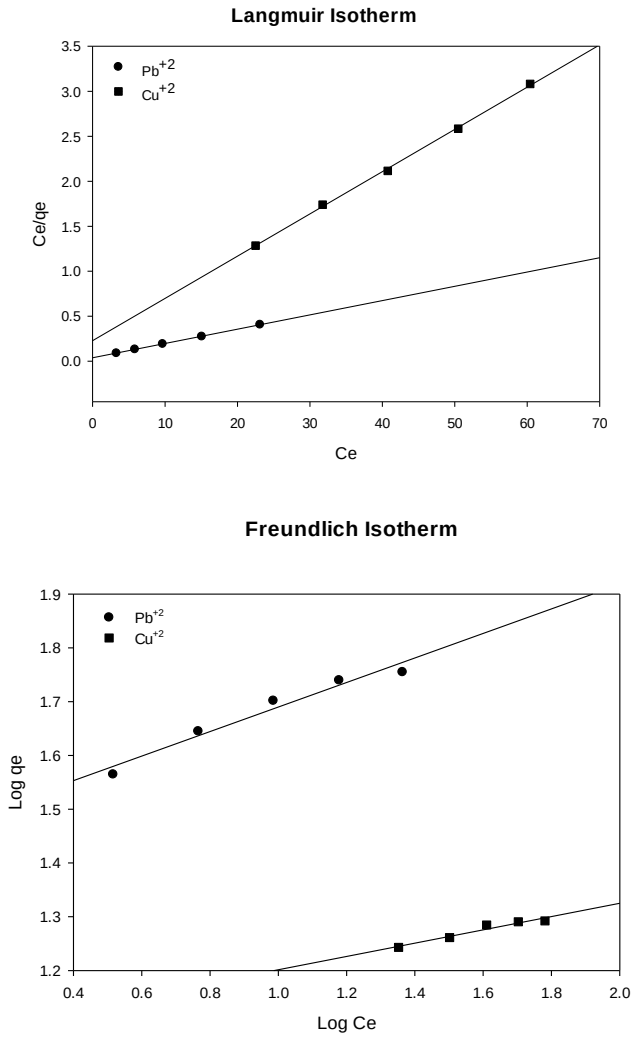

Figure 7. Langmuir and Freundlich isotherms plots for Pb(II) and Cu(II) sorption onto red algae.

3.7. Adsorption Kinetic Study

In this study, four different kinetics models were investigated, namely the pseudo-first order, the pseudo-second order, and the Elovich and the intra-particle diffusion kinetic models, to test the experimental data. The parameters for each kinetic model and its respected correlation coefficients (R^2) are shown in Table 9. Plots of the four kinetic models are shown in Figure 8. The experimental results fitted well with the pseudo-second order model, with the correlation of the coefficient close to unity.

Table 9. The pseudo-first order, pseudo-second order, and Elovich and intra-particle diffusion kinetic parameters for biosorption of Pb(II) and Cu(II) onto *G. changii*.

Model	Equation	Parameters	Pb(II)	Cu(II)
Pseudo-first order	$\log(q_e - q_t) = \log(q_e) - k_1 t$	q_e (mg/g) k_1 (1/min) R^2	14.3152 0.0392 0.9033	17.4 0.04 0.9024
Pseudo-second order	$\frac{t}{q_t} = \frac{1}{q_e K_2} + \frac{1}{q_e}\, t$	q_e (mg/g) k_2 (g/(min·mg)) R^2	40.322 0.366 0.9985	20.04 0.148 0.9976
Elovich kinetic model	$q_t = \frac{1}{\beta} \ln \alpha\beta + \frac{1}{\beta} \ln t$	α β R^2	16.385 0.1659 0.8828	10.536 0.258 0.9901
Intra-particle diffusion	$q_t = k_i t^{0.5} + C$	C k_i (mg/(g·min$^{0.5}$)) R^2	21.827 2.7288 0.7646	5.9639 1.8402 0.9425

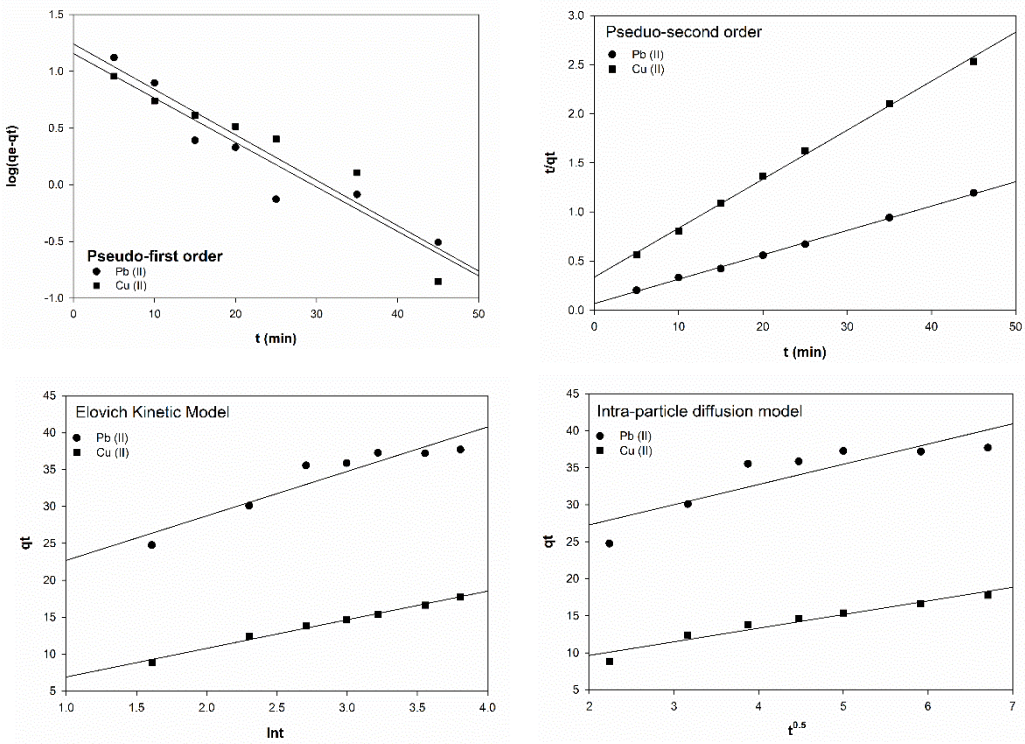

Figure 8. Linear fitting of biosorption of Pb(II) and Cu(II) by *G. changii* to the pseudo-first order, pseudo-second order, and Elovich and intra-particle diffusion kinetic models.

4. Conclusions

Batch sorption experiments were conducted using red algae as a biosorbent for Pb(II) and Cu(II) ions. The effect of solution pH on the removal percentage was studied. The optimum solution pH

values were determined as 4.5 and 5 for Pb(II) and Cu(II), respectively. In addition, RSM was applied to determine the optimum values of initial ion concentration, contact time, and biosorbent dosage to maximise the responses. The optimum conditions for removal of Pb(II) and Cu(II) included the following: initial concentration of 40 mg/L, contact time of 115 and 45 min, and adsorbent dosage of 1 g/L, under which 96.3% and 44.77% removal percentages were achieved, respectively. The adsorption isotherms best fitted the Langmuir model. The adsorption kinetics best fitted the pseudo-second order model. Hence, red alga biomass exhibits huge potential as a cheap and locally available biosorbent for removal of metal ions from industrial wastewater.

Supplementary Materials: The following are available online at http://www.mdpi.com/2073-4441/11/11/2325/s1, Figure S1: EDX element maps of G. *changii* before biosorption, Figure S2: EDX element maps of G. *changii* after Pb(II) biosorption, Figure S3: EDX element maps of G. *changii* after Cu(II) biosorption.

Author Contributions: Formal analysis, M.I.; Funding acquisition, L.B. and S.R.M.K.; Investigation, M.I.; Methodology, M.I.; Project administration, L.B.; Supervision, L.B. and S.R.M.K.; Validation, M.I.; Writing—original draft, M.I.; Writing—review and editing, M.I., L.B., S.R.M.K., and S.Y.

Funding: This research was funded by the STIRF (grant number 0153AA-D76) and YUTP (grant number 0153AA-H32), Universiti Teknologi PETRONAS, Malaysia.

Acknowledgments: We sincerely appreciate Universiti Teknologi PETRONAS and Fishery Department of Langkawi for their strong support in this study.

Conflicts of Interest: The authors declare no conflict of interest.

References

1. Kim, J.-J.; Kim, Y.-S.; Kumar, V. Heavy metal toxicity: An update of chelating therapeutic strategies. *J. Trace Elem. Med. Biol.* **2019**, *54*, 226–231. [CrossRef] [PubMed]
2. Jaishankar, M.; Tseten, T.; Anbalagan, N.; Mathew, B.B.; Beeregowda, K.N. Toxicity, mechanism and health effects of some heavy metals. *Interdiscip. Toxicol.* **2014**, *7*, 60–72. [CrossRef] [PubMed]
3. Abadin, H.; Ashizawa, A.; Stevens, Y.-W.; Llados, F.; Diamond, G.; Sage, G.; Citra, M.; Quinones, A.; Bosch, S.J.; Swarts, S.G. *Toxicological Profile for Lead*; Agency for Toxic Substances and Disease Registry: Atlanta, GA, USA, 2007; p. 582.
4. Griswold, W.; Martin, S. Human Health Effects of Heavy Metals. *Environ. Sci. Technol.* **2009**, *15*, 1–6. Available online: http://www.ncdsupport.net/cms/wp-content/uploads/2015/01/15HumanHealthEffectsofHeavyMetals.pdf (accessed on 20 August 2019).
5. Blázquez, G.; Martín-Lara, M.A.; Tenorio, G.; Calero, M. Batch biosorption of lead (II) from aqueous solutions by olive tree pruning waste: Equilibrium, kinetics and thermodynamic study. *Chem. Eng. J.* **2011**, *168*, 170–177. [CrossRef]
6. Verma, A.; Kumar, S.; Kumar, S. Biosorption of lead ions from the aqueous solution by Sargassum filipendula: Equilibrium and kinetic studies. *J. Environ. Chem. Eng.* **2016**, *4*, 4587–4599. [CrossRef]
7. Nagajyoti, P.C.; Lee, K.D.; Sreekanth, T.V.M. Heavy metals, occurrence and toxicity for plants: A review. *Environ. Chem. Lett.* **2010**, *8*, 199–216. [CrossRef]
8. Tchounwou, P.B.; Yedjou, C.G.; Patlolla, A.K.; Sutton, D.J. Heavy Metal Toxicity and the Environment. In *Molecular, Clinical and Environmental Toxicology: Volume 3: Environmental Toxicology*; Luch, A., Ed.; Springer: Basel, Switzerland, 2012; pp. 133–164. ISBN 978-3-7643-8340-4.
9. Vareda, J.P.; Valente, A.J.M.; Durães, L. Assessment of heavy metal pollution from anthropogenic activities and remediation strategies: A review. *J. Environ. Manag.* **2019**, *246*, 101–118. [CrossRef]
10. Yahya, M.A.; Al-Qodah, Z.; Ngah, C.W.Z. Agricultural bio-waste materials as potential sustainable precursors used for activated carbon production: A review. *Renew. Sustain. Energy Rev.* **2015**, *46*, 218–235. [CrossRef]
11. Lesmana, S.O.; Febriana, N.; Soetaredjo, F.E.; Sunarso, J.; Ismadji, S. Studies on potential applications of biomass for the separation of heavy metals from water and wastewater. *Biochem. Eng. J.* **2009**, *44*, 19–41. [CrossRef]
12. Zhou, P.; Huang, J.-C.; Li, A.W.F.; Wei, S. Heavy metal removal from wastewater in fluidized bed reactor. *Water Res.* **1999**, *33*, 1918–1924. [CrossRef]

13. Fu, F.; Wang, Q. Removal of heavy metal ions from wastewaters: A review. *J. Environ. Manag.* **2011**, *92*, 407–418. [CrossRef] [PubMed]
14. Volesky, B. Biosorption and me. *Water Res.* **2007**, *41*, 4017–4029. [CrossRef] [PubMed]
15. Jun, B.M.; Kim, S.; Kim, Y.; Her, N.; Heo, J.; Han, J.; Jang, M.; Park, C.M.; Yoon, Y. Comprehensive evaluation on removal of lead by graphene oxide and metal organic framework. *Chemosphere* **2019**, *231*, 82–92. [CrossRef] [PubMed]
16. Hong, M.; Yu, L.; Wang, Y.; Zhang, J.; Chen, Z.; Dong, L.; Zan, Q.; Li, R. Heavy metal adsorption with zeolites: The role of hierarchical pore architecture. *Chem. Eng. J.* **2019**, *359*, 363–372. [CrossRef]
17. Li, Y.; Bai, P.; Yan, Y.; Yan, W.; Shi, W.; Xu, R. Removal of Zn^{2+}, Pb^{2+}, Cd^{2+}, and Cu^{2+} from aqueous solution by synthetic clinoptilolite. *Microporous Mesoporous Mater.* **2019**, *273*, 203–211. [CrossRef]
18. Park, C.M.; Han, J.; Chu, K.H.; Al-Hamadani, Y.A.J.; Her, N.; Heo, J.; Yoon, Y. Influence of solution pH, ionic strength, and humic acid on cadmium adsorption onto activated biochar: Experiment and modeling. *J. Ind. Eng. Chem.* **2017**, *48*, 186–193. [CrossRef]
19. Jun, B.-M.; Kim, S.; Heo, J.; Park, C.M.; Her, N.; Jang, M.; Huang, Y.; Han, J.; Yoon, Y. Review of MXenes as new nanomaterials for energy storage/delivery and selected environmental applications. *Nano Res.* **2019**, *12*, 471–487. [CrossRef]
20. Fiyadh, S.S.; AlSaadi, M.A.; Jaafar, W.Z.; AlOmar, M.K.; Fayaed, S.S.; Mohd, N.S.; Hin, L.S.; El-Shafie, A. Review on heavy metal adsorption processes by carbon nanotubes. *J. Clean. Prod.* **2019**, *230*, 783–793. [CrossRef]
21. Marciniak, M.; Goscianska, J.; Frankowski, M.; Pietrzak, R. Optimal synthesis of oxidized mesoporous carbons for the adsorption of heavy metal ions. *J. Mol. Liq.* **2019**, *276*, 630–637. [CrossRef]
22. Sarı, A.; Tuzen, M.; Uluözlü, Ö.D.; Soylak, M. Biosorption of Pb(II) and Ni(II) from aqueous solution by lichen (Cladonia furcata) biomass. *Biochem. Eng. J.* **2007**, *37*, 151–158. [CrossRef]
23. Joseph, L.; Jun, B.-M.; Flora, J.R.V.; Park, C.M.; Yoon, Y. Removal of heavy metals from water sources in the developing world using low-cost materials: A review. *Chemosphere* **2019**, *229*, 142–159. [CrossRef] [PubMed]
24. Bilal, M.; Rasheed, T.; Sosa-Hernández, J.; Raza, A.; Nabeel, F.; Iqbal, H. Biosorption: An Interplay between Marine Algae and Potentially Toxic Elements—A Review. *Mar. Drugs* **2018**, *16*, 65. [CrossRef] [PubMed]
25. Bailey, S.E.; Olin, T.J.; Bricka, R.M.; Adrian, D.D. A review of potentially low-cost sorbents for heavy metals. *Water Res.* **1999**, *33*, 2469–2479. [CrossRef]
26. Hamdy, A.A. Biosorption of heavy metals by marine algae. *Curr. Microbiol.* **2000**, *41*, 232–238. [CrossRef] [PubMed]
27. Deniz, F.; Ersanli, E.T. An ecofriendly approach for bioremediation of contaminated water environment: Potential contribution of a coastal seaweed community to environmental improvement. *Int. J. Phytoremediat.* **2018**, *20*, 256–263. [CrossRef]
28. Vafajoo, L.; Cheraghi, R.; Dabbagh, R.; McKay, G. Removal of cobalt (II) ions from aqueous solutions utilizing the pre-treated 2-Hypnea Valentiae algae: Equilibrium, thermodynamic, and dynamic studies. *Chem. Eng. J.* **2018**, *331*, 39–47. [CrossRef]
29. Santos, S.C.R.; Ungureanu, G.; Volf, I.; Boaventura, R.A.R.; Botelho, C.M.S. Macroalgae Biomass as Sorbent for Metal Ions. In *Biomass as Renewable Raw Material to Obtain Bioproducts of High-Tech Value*; Elsevier: Amsterdam, The Netherlands, 2018; pp. 69–112. ISBN 9780444637970.
30. Cheng, S.Y.; Show, P.-L.; Lau, B.F.; Chang, J.-S.; Ling, T.C. New Prospects for Modified Algae in Heavy Metal Adsorption. *Trends Biotechnol.* **2019**, 1–14, in press. [CrossRef]
31. Wang, J.; Chen, C. Biosorbents for heavy metals removal and their future. *Biotechnol. Adv.* **2009**, *27*, 195–226. [CrossRef]
32. Johnston, E.T.J.; Lim, P.E.; Buhari, N.; Keil, E.J.; Djawad, M.I.; Vis, M.L. Diversity of freshwater red algae (Rhodophyta) in Malaysia and Indonesia from morphological and molecular data. *Phycologia* **2014**, *53*, 329–341. [CrossRef]
33. Norziah, M.H.; Ching, C.Y. Nutritional Composition of Edible SeaweedGracilaria Changgi. *Food Chem.* **2000**, *68*, 69–76. [CrossRef]
34. Phang, S.-M.; Shaharuddin, S.; Noraishah, H.; Sasekumar, A. Studies on Gracilaria changii (Gracilariales, Rhodophyta) from Malaysian mangroves. *Hydrobiologia* **1996**, *326*, 347–352. [CrossRef]

35. Zhu, X.; Gao, Y.; Yue, Q.; Kan, Y.; Kong, W.; Gao, B. Preparation of green alga-based activated carbon with lower impregnation ratio and less activation time by potassium tartrate for adsorption of chloramphenicol. *Ecotoxicol. Environ. Saf.* **2017**, *145*, 289–294. [CrossRef] [PubMed]
36. Van Thuan, T.; Quynh, B.T.P.; Nguyen, T.D.; Ho, V.T.T.; Bach, L.G. Response surface methodology approach for optimization of Cu^{2+}, Ni^{2+} and Pb^{2+}adsorption using KOH^{-} activated carbon from banana peel. *Surf. Interfaces* **2017**, *6*, 209–217. [CrossRef]
37. Witek-Krowiak, A.; Chojnacka, K.; Podstawczyk, D.; Dawiec, A.; Pokomeda, K. Application of response surface methodology and artificial neural network methods in modelling and optimization of biosorption process. *Bioresour. Technol.* **2014**, *160*, 150–160. [CrossRef]
38. Lingamdinne, L.P.; Koduru, J.R.; Chang, Y.Y.; Karri, R.R. Process optimization and adsorption modeling of Pb(II) on nickel ferrite-reduced graphene oxide nano-composite. *J. Mol. Liq.* **2018**, *250*, 202–211. [CrossRef]
39. Xia, Y.; Yang, T.; Zhu, N.; Li, D.; Chen, Z.; Lang, Q.; Liu, Z.; Jiao, W. Enhanced adsorption of Pb(II) onto modified hydrochar: Modeling and mechanism analysis. *Bioresour. Technol.* **2019**, *288*, 1–8. [CrossRef]
40. John Babu, D.; King, P.; Prasanna Kumar, Y. Optimization of Cu(II) biosorption onto sea urchin test using response surface methodology and artificial neural networks. *Int. J. Environ. Sci. Technol.* **2019**, *16*, 1885–1896. [CrossRef]
41. Nishikawa, E.; da Silva, M.G.C.; Vieira, M.G.A. Cadmium biosorption by alginate extraction waste and process overview in Life Cycle Assessment context. *J. Clean. Prod.* **2018**, *178*, 166–175. [CrossRef]
42. Yari, M.; Rajabi, M.; Moradi, O.; Yari, A.; Asif, M.; Agarwal, S.; Gupta, V.K. Kinetics of the adsorption of Pb(II) ions from aqueous solutions by graphene oxide and thiol functionalized graphene oxide. *J. Mol. Liq.* **2015**, *209*, 50–57. [CrossRef]
43. Zhang, X.; Cheng, C.; Zhao, J.; Ma, L.; Sun, S.; Zhao, C. Polyethersulfone enwrapped graphene oxide porous particles for water treatment. *Chem. Eng. J.* **2013**, *215–216*, 72–81. [CrossRef]
44. Li, Y.; Du, Q.; Liu, T.; Peng, X.; Wang, J.; Sun, J.; Wang, Y.; Wu, S.; Wang, Z.; Xia, Y.; et al. Comparative study of methylene blue dye adsorption onto activated carbon, graphene oxide, and carbon nanotubes. *Chem. Eng. Res. Des.* **2013**, *91*, 361–368. [CrossRef]
45. Peng, S.H.; Wang, R.; Yang, L.Z.; He, L.; He, X.; Liu, X. Biosorption of copper, zinc, cadmium and chromium ions from aqueous solution by natural foxtail millet shell. *Ecotoxicol. Environ. Saf.* **2018**, *165*, 61–69. [CrossRef] [PubMed]
46. Oliveira, R.C.; Hammer, P.; Guibal, E.; Taulemesse, J.M.; Garcia, O. Characterization of metal-biomass interactions in the lanthanum (III) biosorption on Sargassum sp. using SEM/EDX, FTIR, and XPS: Preliminary studies. *Chem. Eng. J.* **2014**, *239*, 381–391. [CrossRef]
47. Yuan, W.; Cheng, J.; Huang, H.; Xiong, S.; Gao, J.; Zhang, J.; Feng, S. Optimization of cadmium biosorption by Shewanella putrefaciens using a Box-Behnken design. *Ecotoxicol. Environ. Saf.* **2019**, *175*, 138–147. [CrossRef] [PubMed]
48. Do Nascimento, J.M.; de Oliveira, J.D.; Rizzo, A.C.L.; Leite, S.G.F. Biosorption Cu(II) by the yeast Saccharomyces cerevisiae. *Biotechnol. Rep.* **2019**, *21*, e00315. [CrossRef]
49. Daneshvar, E.; Vazirzadeh, A.; Niazi, A.; Sillanpää, M.; Bhatnagar, A. A comparative study of methylene blue biosorption using different modified brown, red and green macroalgae–Effect of pretreatment. *Chem. Eng. J.* **2017**, *307*, 435–446. [CrossRef]
50. Coates, J. Interpretation of infrared spectra, a practical approach. In *Encyclopedia of Analytical Chemistry*; Meyers, R.A., McKelvy, M.L., Eds.; John Wiley & Sons: Chichester, UK, 2000. [CrossRef]
51. Li, Y.; Song, S.; Xia, L.; Yin, H.; García Meza, J.V.; Ju, W. Enhanced Pb(II) removal by algal-based biosorbent cultivated in high-phosphorus cultures. *Chem. Eng. J.* **2019**, *361*, 167–179. [CrossRef]
52. El Azm, N.A.; Fleita, D.; Rifaat, D.; Mpingirika, E.Z.; Amleh, A.; El-Sayed, M.M.H. Production of bioactive compounds from the sulfated polysaccharides extracts of ulva lactuca: Post-extraction enzymatic hydrolysis followed by ion-exchange chromatographic fractionation. *Molecules* **2019**, *24*, 1–17. [CrossRef]
53. Cardoso, I.; Rodrigues, A.; Ferreira, D. Extraction and Analysis of Compounds with Antibacterial Potential from the Red Alga Grateloupia turuturu. *J. Mar. Sci. Eng.* **2019**, *7*, 220. [CrossRef]
54. Pavasant, P.; Apiratikul, R.; Sungkhum, V.; Suthiparinyanont, P.; Wattanachira, S.; Marhaba, T.F. Biosorption of Cu^{2+}, Cd^{2+}, Pb^{2+}, and Zn^{2+} using dried marine green macroalga Caulerpa lentillifera. *Bioresour. Technol.* **2006**, *97*, 2321–2329. [CrossRef]

55. Ibrahim, W.M. Biosorption of heavy metal ions from aqueous solution by red macroalgae. *J. Hazard. Mater.* **2011**, *192*, 1827–1835. [CrossRef] [PubMed]
56. Ibrahim, W.M.; Hassan, A.F.; Azab, Y.A. Biosorption of toxic heavy metals from aqueous solution by Ulva lactuca activated carbon. *Egypt. J. Basic Appl. Sci.* **2016**, *3*, 241–249. [CrossRef]
57. Sheng, P.X.; Ting, Y.P.; Chen, J.P.; Hong, L. Sorption of lead, copper, cadmium, zinc, and nickel by marine algal biomass: Characterization of biosorptive capacity and investigation of mechanisms. *J. Colloid Interface Sci.* **2004**, *275*, 131–141. [CrossRef] [PubMed]
58. Jalali, R.; Ghafourian, H.; Asef, Y.; Davarpanah, S.J.; Sepehr, S. Removal and recovery of lead using nonliving biomass of marine algae. *J. Hazard. Mater.* **2002**, *92*, 253–262. [CrossRef]
59. Hu, X.J.; Liu, Y.G.; Wang, H.; Zeng, G.M.; Hu, X.; Guo, Y.M.; Li, T.T.; Chen, A.W.; Jiang, L.H.; Guo, F.Y. Adsorption of copper by magnetic graphene oxide-supported β-cyclodextrin: Effects of pH, ionic strength, background electrolytes, and citric acid. *Chem. Eng. Res. Des.* **2015**, *93*, 675–683. [CrossRef]
60. Sulaymon, A.H.; Mohammed, A.A.; Al-Musawi, T.J. Competitive biosorption of lead, cadmium, copper, and arsenic ions using algae. *Environ. Sci. Pollut. Res.* **2013**, *20*, 3011–3023. [CrossRef]
61. Lee, Y.C.; Chang, S.P. The biosorption of heavy metals from aqueous solution by Spirogyra and Cladophora filamentous macroalgae. *Bioresour. Technol.* **2011**, *102*, 5297–5304. [CrossRef]
62. Vilar, V.J.P.; Botelho, C.M.S.; Pinheiro, J.P.S.; Domingos, R.F.; Boaventura, R.A.R. Copper removal by algal biomass: Biosorbents characterization and equilibrium modelling. *J. Hazard. Mater.* **2009**, *163*, 1113–1122. [CrossRef]
63. Mahmood, T.; Ali, R.; Naeem, A.; Hamayun, M.; Aslam, M. Potential of used Camellia sinensis leaves as precursor for activated carbon preparation by chemical activation with H3PO4; optimization using response surface methodology. *Process Saf. Environ. Prot.* **2017**, *109*, 548–563. [CrossRef]
64. Yavari, S.; Malakahmad, A.; Sapari, N.B. Effects of production conditions on yield and physicochemical properties of biochars produced from rice husk and oil palm empty fruit bunches. *Environ. Sci. Pollut. Res.* **2016**, *23*, 17928–17940. [CrossRef]
65. Mondal, N.K.; Samanta, A.; Roy, P.; Das, B. Optimization study of adsorption parameters for removal of Cr (VI) using Magnolia leaf biomass by response surface methodology. *Sustain. Water Resour. Manag.* **2019**, 1–13. [CrossRef]
66. Roy, P.; Dey, U.; Chattoraj, S.; Mukhopadhyay, D.; Mondal, N.K. Modeling of the adsorptive removal of arsenic (III) using plant biomass: A bioremedial approach. *Appl. Water Sci.* **2017**, *7*, 1307–1321. [CrossRef]
67. Sarada, B.; Prasad, M.K.; Kumar, K.K.; Ramachandra Murthy, C.V. Cadmium removal by macro algae Caulerpa fastigiata: Characterization, kinetic, isotherm and thermodynamic studies. *J. Environ. Chem. Eng.* **2014**, *2*, 1533–1542. [CrossRef]
68. Hashim, M.A.; Chu, K.H. Biosorption of cadmium by brown, green, and red seaweeds. *Chem. Eng. J.* **2004**, *97*, 249–255. [CrossRef]
69. Romera, E.; González, F.; Ballester, A.; Blázquez, M.L.; Muñoz, J.A. Comparative study of biosorption of heavy metals using different types of algae. *Bioresour. Technol.* **2007**, *98*, 3344–3353. [CrossRef]
70. Momčilović, M.; Purenović, M.; Bojić, A.; Zarubica, A.; Ranđelović, M. Removal of lead (II) ions from aqueous solutions by adsorption onto pine cone activated carbon. *Desalination* **2011**, *276*, 53–59. [CrossRef]

© 2019 by the authors. Licensee MDPI, Basel, Switzerland. This article is an open access article distributed under the terms and conditions of the Creative Commons Attribution (CC BY) license (http://creativecommons.org/licenses/by/4.0/).